



# CHORUS

This is the accepted manuscript made available via CHORUS. The article has been published as:

## Ultrafast electron-lattice coupling dynamics in $\text{VO}_{\{2\}}$ and $\text{V}_{\{2\}}\text{O}_{\{3\}}$ thin films

Elsa Abreu, Stephanie N. Gilbert Corder, Sun Jin Yun, Siming Wang, Juan Gabriel Ramírez, Kevin West, Jingdi Zhang, Salinporn Kittiwatanakul, Ivan K. Schuller, Jiwei Lu, Stuart A.

Wolf, Hyun-Tak Kim, Mengkun Liu, and Richard D. Averitt

Phys. Rev. B **96**, 094309 — Published 21 September 2017

DOI: [10.1103/PhysRevB.96.094309](https://doi.org/10.1103/PhysRevB.96.094309)

# Ultrafast Electron-Lattice Coupling Dynamics in VO<sub>2</sub> and V<sub>2</sub>O<sub>3</sub> Thin Films

Elsa Abreu,<sup>1,2,\*</sup> Stephanie N. Gilbert Corder,<sup>1,3</sup> Sun Jin Yun,<sup>4,5</sup> Siming Wang,<sup>6,7,8,9</sup> Juan Gabriel Ramírez,<sup>10</sup> Kevin West,<sup>11,6,7</sup> Jingdi Zhang,<sup>6,†</sup> Salinporn Kittiwatanakul,<sup>11</sup> Ivan K. Schuller,<sup>6,7,8</sup> Jiwei Lu,<sup>11</sup> Stuart A. Wolf,<sup>11,12</sup> Hyun-Tak Kim,<sup>4,5</sup> Mengkun Liu,<sup>3,‡</sup> and Richard D. Averitt<sup>6,§</sup>

<sup>1</sup>*Both authors contributed equally to this work.*

<sup>2</sup>*Institute for Quantum Electronics, Department of Physics,  
ETH Zurich, 8093 Zurich, Switzerland*

<sup>3</sup>*Department of Physics and Astronomy,  
Stony Brook University, New York, 11794*

<sup>4</sup>*Metal-Insulator Transition Lab, ETRI, Daejeon 305-350, South Korea*

<sup>5</sup>*School of Advanced Device Technology,  
University of Science and Technology, Daejeon 305-333, South Korea*

<sup>6</sup>*Department of Physics, The University of California  
at San Diego, La Jolla, California 92093, USA*

<sup>7</sup>*Center for Advanced Nanoscience,  
The University of California at San Diego, La Jolla, California 92093, USA*

<sup>8</sup>*Materials Science and Engineering Program,  
The University of California at San Diego, La Jolla, California 92093, USA*

<sup>9</sup>*Materials Sciences Division, Lawrence Berkeley  
National Laboratory, Berkeley, California 94720, USA*

<sup>10</sup>*Department of Physics, Universidad de los Andes, Bogotá 111711, Colombia*

<sup>11</sup>*Department of Materials Science and Engineering,  
University of Virginia, Charlottesville VA 22904, USA*

<sup>12</sup>*Department of Physics, University of Virginia, Charlottesville VA 22904, USA*

(Dated: July 28, 2017; Received)

## Abstract

Ultrafast optical pump - optical probe and optical pump - terahertz probe spectroscopy were performed on vanadium dioxide ( $\text{VO}_2$ ) and vanadium sesquioxide ( $\text{V}_2\text{O}_3$ ) thin films over a wide temperature range. A comparison of the experimental data from these two different techniques and two different vanadium oxides, in particular a comparison of the spectral weight oscillations generated by the photoinduced longitudinal acoustic modulation, reveals the strong electron-phonon coupling that exists in both materials. The low energy Drude response of  $\text{V}_2\text{O}_3$  appears more amenable than  $\text{VO}_2$  to ultrafast strain control. Additionally, our results provide a measurement of the temperature dependence of the sound velocity in both systems, revealing a four- to fivefold increase in  $\text{VO}_2$  and a three- to fivefold increase in  $\text{V}_2\text{O}_3$  across the insulator-to-metal phase transition. Our data also confirm observations of strong damping and phonon anharmonicity in the metallic phase of  $\text{VO}_2$ , and suggest that a similar phenomenon might be at play in the metallic phase of  $\text{V}_2\text{O}_3$ . More generally, our simple table-top approach provides relevant and detailed information about dynamical lattice properties of vanadium oxides, paving the way to similar studies in other complex materials.

## I. INTRODUCTION

Vanadium oxides are well known examples of materials where the phases are determined by strong interactions between different degrees of freedom. Such complex systems, where charge, lattice, orbital, and spin contributions can be equally strong and are frequently coupled, exhibit a variety of phenomena including high temperature superconductivity<sup>1</sup>, colossal magnetoresistance<sup>2</sup>, multiferroicity<sup>3</sup>, and topological surface states<sup>4</sup>. Given the complex nature of these materials, the various phases are generally challenging to investigate experimentally. Ultrafast time-resolved techniques are a successful route to approach this problem<sup>5,6</sup>. In particular, time-resolved measurements in different energy ranges have contributed to the understanding of insulator-to-metal transitions (IMTs) in vanadium dioxide ( $\text{VO}_2$ ) and vanadium sesquioxide ( $\text{V}_2\text{O}_3$ ) as a function of temperature, pressure and doping<sup>7-15</sup>. These measurements have also shed light onto the nature of the different insulating phases in both systems<sup>8,16-18</sup>, and onto the electron-phonon coupling driven acoustic response in  $\text{V}_2\text{O}_3$ <sup>8,9</sup>.

Despite many ultrafast and static measurements, the exact mechanisms responsible for the IMTs in vanadium oxides and especially in  $\text{VO}_2$  remain widely debated<sup>19-27</sup>, namely the contribution of electronic correlations (Mott-Hubbard picture) and of electron-lattice mediated effects (Peierls model)<sup>17,23,28-30</sup>. It is clear, however, that multiple pathways are possible to initiate pressure and temperature dependent transitions, and that electronic and lattice effects are strongly coupled<sup>17,28,31,32</sup>. Measurements that dynamically investigate this coupling are therefore essential to assist in understanding the nature of IMTs, **which serves as the primary motivation for the present work.**

Bulk  $\text{VO}_2$  undergoes an IMT at 340 K, along with a monoclinic-to-rutile structural transition<sup>19,33</sup> (cf. phase diagram in Fig. S1a<sup>34</sup>). In the low temperature phase, the vanadium ions dimerize and tilt to form a nonmagnetic insulator<sup>23</sup>. Above-bandgap photoexcitation of the monoclinic insulator can promote electrons to anti-bonding states, causing repulsion between the dimerized vanadium ions and lattice expansion, followed by long-range shear rearrangements at the speed of sound<sup>18,22</sup>. Above a critical fluence threshold the metallic phase forms via nucleation and growth<sup>17,30,35,36</sup>. The acoustic and optical phonon landscape changes drastically across the IMT, and phonons have recently been seen to account for 2/3 of the entropy increase at the IMT and to stabilize the metallic phase<sup>26,28</sup>. These observations suggest that lattice effects play a significant role in driving the IMT in

VO<sub>2</sub>. Our experiments access the coupling between lattice and electronic properties, highlighting the important role played by the structure in determining the dynamic electronic response of VO<sub>2</sub>.

V<sub>2</sub>O<sub>3</sub> is a low temperature monoclinic antiferromagnetic insulator which transitions to a paramagnetic rhombohedral metal above 155 K<sup>19,37</sup> (cf. phase diagram in Fig. S1b<sup>34</sup>). Initial reports stated that the system exhibits a classical Mott-Hubbard transition where electrons localize to form the insulating phase<sup>20,21</sup>. However, more recent work points to electron-lattice effects contributing strongly to the first order IMT in the undoped compound<sup>24</sup>, and questions the equivalence of temperature and pressure routes in driving the phase transition in doped V<sub>2</sub>O<sub>3</sub><sup>10</sup>. The strong strain-dependence of metallic V<sub>2</sub>O<sub>3</sub> manifests via the large influence of ultrafast acoustic modulations on the spectral weight redistribution dynamics, particularly in the far infrared region of the spectra corresponding to the low energy Drude weight<sup>9</sup>. As with VO<sub>2</sub>, our experimental results on V<sub>2</sub>O<sub>3</sub> enhance the understanding of the role of the lattice in determining the electronic properties and dynamics, and further, they enable a direct comparison between the two materials.

We therefore present a comparative ultrafast pump-probe study of photoinduced acoustic effects in VO<sub>2</sub> and V<sub>2</sub>O<sub>3</sub>, seen in both optical reflectivity and terahertz (THz) conductivity dynamics. Transient reflectivity measurements at 1.55 eV are sensitive to interband transitions in VO<sub>2</sub> and V<sub>2</sub>O<sub>3</sub>, with insulating gaps of 0.6 eV and 0.5 eV, respectively<sup>23</sup>, while THz probes the quasiparticle dynamics, effectively yielding a dynamical measurement of the dc conductivity.

Our main conclusions are that (i) both VO<sub>2</sub> and V<sub>2</sub>O<sub>3</sub> exhibit significant electron-phonon coupling, with V<sub>2</sub>O<sub>3</sub> being significantly more amenable than VO<sub>2</sub> to Drude weight modulation; (ii) the acoustic signatures we observe appear to be quite robust against variations in crystallinity in the different thin film samples under study; (iii) sound velocity increases by over a factor of three across the insulator-to-metal transition for both VO<sub>2</sub> and V<sub>2</sub>O<sub>3</sub> thin films; and (iv) acoustic damping increases in both metallic phases, suggesting phonon entropy as a significant stabilization mechanism in both VO<sub>2</sub> and V<sub>2</sub>O<sub>3</sub>.

First, our results show that similar to V<sub>2</sub>O<sub>3</sub><sup>8,9</sup>, VO<sub>2</sub> exhibits a modulation of the electronic response due to photoinduced acoustic effects, albeit to a lesser degree. This influence of small structural variations on the electronic behavior attests to significant electron-phonon coupling. In this case electron-phonon coupling refers to the rate at which energy is trans-

ferred between electrons and phonon modes of the lattice as used in the two-temperature model<sup>34,38</sup>, rather than to a strictly microscopic parameter. Second, thin film samples with varying **crystallinity** exhibit different static and dynamic electronic responses. **Variations in morphology and crystallinity are widely reported for thin films samples of vanadium oxides, due to e.g. strain, mismatch with the substrate and growth conditions. They translate into a significant density of defects in the system, mostly structural in nature but potentially including oxygen vacancies as well, which have a strong and distinct influence on the electronic response.**<sup>32,36,39</sup> Thin films with fewer defects have properties closer to bulk and are therefore characterized by a larger THz conductivity in the metallic state and by larger photoinduced conductivity variations. **Variations in the static metallic phase conductivity enable us to indirectly compare defect densities in the different thin films under study, since a direct quantification of defects is extremely challenging to obtain.** In contrast to **the changes in the static** electronic behavior, the **dynamic** acoustic signatures we observe appear to be quite robust against varying defect density in the thin films. Third, our data provide a temperature dependent measure of the sound velocity in both VO<sub>2</sub> and V<sub>2</sub>O<sub>3</sub> **thin films**, revealing an increase in the sound velocity across the insulator-to-metal transition, four- to fivefold for VO<sub>2</sub> and three- to fivefold for V<sub>2</sub>O<sub>3</sub>, **i.e. significantly larger (>2x) than reported previously in bulk single crystals**<sup>26,40</sup>. Finally, we verify that acoustic damping increases in the metallic phase of VO<sub>2</sub>, compared to the insulating phase, in agreement with previous reports that present phonon entropy as a stabilization mechanism for the metallic phase<sup>28</sup>. V<sub>2</sub>O<sub>3</sub> exhibits a similarly increased damping in the metallic phase, hinting that phonon anharmonicity might also be much stronger than in the insulating phase, and that phonon effects might play a significant role in the IMT of this material as well.

## II. EXPERIMENTAL METHODS

Transient optical reflectivity measurements were performed using 35 fs pulses at 800 nm (1.55 eV) from a 1 KHz repetition rate, 3 W average power Ti:sapphire regenerative amplifier. Pump and probe fluences were set at 1-4 mJ/cm<sup>2</sup> and < 10 μJ/cm<sup>2</sup>, respectively. THz pulses 1 ps in duration were generated via optical rectification and detected by electro-optic sampling in ZnTe. In contrast to the optical measurements at 1.55 eV, the THz pulses (0.1 - 2.5 THz) effectively probe the low energy Drude response<sup>23</sup>, which is flat and

devoid of any spectral features in the chosen frequency range. Transient optical reflectivity measurements at 800 nm, yielding  $\Delta R/R$ , and THz conductivity measurements<sup>5</sup>, yielding  $\Delta\sigma$ , were performed in parallel, with the same pump conditions. In both cases pump and probe beams were set at approximately normal incidence to the sample, with a pump focal spot size about ten times larger than that of the probe. The penetration depth of the 1.55 eV pulse is on the order of the sample thickness for the VO<sub>2</sub> and V<sub>2</sub>O<sub>3</sub> thin film samples used in this work (cf. Table SIII in the Supplemental Material<sup>34</sup>). Inhomogeneity in the excited volume is therefore not significant enough to affect the observed dynamics, meaning that both 800 nm and THz probe beams sample similarly excited regions.

Of particular relevance to this work is the ability to generate coherent acoustic phonons using ultrafast optical excitation. The ultrafast above bandgap optical pulse is absorbed near the surface causing a localized temperature increase. Thermal expansion leads to a transient stress which launches a strain wave in the material. The propagating acoustic phonon modifies the frequency dependent refractive index and can therefore be detected optically via modulation of  $\Delta R/R$  at 800 nm, and of  $\Delta\sigma$  around 1 THz. When the film thickness is on the order of the longitudinal acoustic phonon wavelength an acoustic standing wave is generated and detected instead<sup>41</sup>. Analytic<sup>42,43</sup> and conceptual<sup>41</sup> aspects of the generation and detection of coherent acoustic modulations can be found in the literature<sup>41-43</sup>.

Our samples consist of 75 nm and 50 nm thick films of VO<sub>2</sub> on c-cut Al<sub>2</sub>O<sub>3</sub><sup>44</sup>, 75 nm thick films of V<sub>2</sub>O<sub>3</sub> on c-cut Al<sub>2</sub>O<sub>3</sub><sup>45</sup>, and 95 nm thick films of V<sub>2</sub>O<sub>3</sub> on r-cut Al<sub>2</sub>O<sub>3</sub><sup>32</sup>. The VO<sub>2</sub> films have a well defined out of plane rutile c-axis, and three preferred in-plane orientations due to the hexagonal symmetry of the c-cut Al<sub>2</sub>O<sub>3</sub> substrate<sup>46</sup>. The 75 nm V<sub>2</sub>O<sub>3</sub> film has a well-defined rhombohedral out of plane [110] axis but is polycrystalline in plane, while the 95 nm film is nearly single crystalline throughout. **No signatures of other vanadium oxides phases were detected in either of the samples beyond the nominal VO<sub>2</sub> or V<sub>2</sub>O<sub>3</sub>. All films are epitaxial, and** details of the fabrication can be found elsewhere<sup>32,44,45</sup>. Unless otherwise specified, the results presented in this paper correspond to the 75 nm films.

The sample temperature was set using a continuous flow cryostat, pumped down to 10<sup>-6</sup> mbar and equipped with a heating stage.

### III. RESULTS

#### A. Temperature dependent THz conductivity

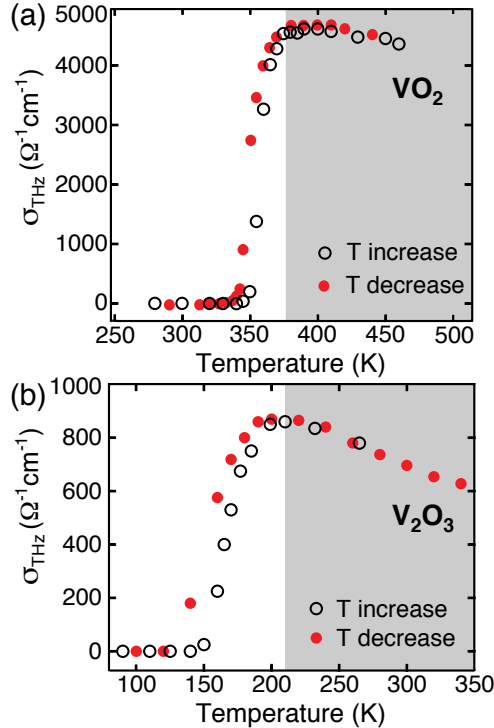


FIG. 1. Temperature dependence of the static far-infrared conductivity for the 75 nm thick (a)  $\text{VO}_2$  and (b)  $\text{V}_2\text{O}_3$  thin films. Open black (solid red) symbols indicate increasing (decreasing) temperature. Both samples display hysteresis, characteristic of first order phase transitions happening at 360 K in  $\text{VO}_2$  and at 160 K in  $\text{V}_2\text{O}_3$ . The fully metallic region is shaded gray.

Figure 1 shows the static THz conductivity of the 75 nm  $\text{VO}_2$  and  $\text{V}_2\text{O}_3$  films measured using THz spectroscopy. Fig. 1a shows that the IMT in the  $\text{VO}_2$  film occurs at  $T_{IMT} = 360$  K, and that a maximum conductivity of  $4800 (\Omega\text{cm})^{-1}$  is obtained at 380 K.  $\text{V}_2\text{O}_3$  is seen from Fig. 1b to have  $T_{IMT} = 160$  K, with a peak conductivity of  $900 (\Omega\text{cm})^{-1}$  at 200 K. These measurements demonstrate that our  $\text{VO}_2$  and  $\text{V}_2\text{O}_3$  films behave similarly to bulk single crystals, which attests to the generality of our conclusions. Above 200 K the  $\text{V}_2\text{O}_3$  metallic state conductivity decreases dramatically (Fig. S1<sup>34</sup>), beyond what would be expected from an increased electron-phonon scattering rate, due to the strongly correlated nature of this “bad” metal region<sup>23,47</sup>. The relative conductivity decrease in the  $\text{VO}_2$  metallic

state above 380 K is smaller compared to  $V_2O_3$ , with a 6% conductivity drop per 50 K for  $VO_2$  and an 11 % conductivity drop per 50 K for  $V_2O_3$ . This is consistent with suggestions that electronic correlations have a smaller impact on the metallic phase of  $VO_2$  compared to metallic  $V_2O_3$ <sup>48,49</sup>, which enters a crossover region to a pure Mott insulator phase above 450 K (Fig. S1<sup>34</sup>). Corresponding temperature-dependent static conductivity data for the 95 nm  $V_2O_3$  film are shown in Fig. S2<sup>34</sup>.

### B. Conductivity and reflectivity dynamics in $VO_2$

Figures 2a, 3a and 3b show the transient conductivity ( $\Delta\sigma$ ) and transient reflectivity at 800 nm ( $\Delta R/R$ ) of  $VO_2$  at low (Fig. 2a) and high (Figs. 3a and 3b) initial temperatures for a pump fluence of 3.8 mJ/cm<sup>2</sup>. From the conductivity dynamics at  $T < T_{IMT}$ , shown in Fig. 2a, it is clear that the maximum value achieved for the transient conductivity  $\Delta\sigma(t)$  increases with initial temperature. Also, for  $T = 77$  K,  $\Delta\sigma(t)$  recovers in less than 10 ps, whereas for  $T > 160$  K the deposited energy is sufficient to thermally stabilize the metallic phase beyond our 350 ps measurement window<sup>34</sup>. As previously observed, the tens of ps timescale for the conductivity increase is considerably larger than the <1 ps electron-phonon thermalization time (Fig. S7<sup>34</sup>) due to the nucleation and growth process that accompanies the IMT<sup>35,50</sup>.

For  $T > T_{IMT}$  the metallic phase dominates the transient photothermal response of  $VO_2$ .  $\Delta\sigma$ , shown in Fig. 3a, decreases following photoexcitation in agreement with Fig. 1a, and so does  $\Delta R/R$  (Fig. 3b). Most significantly, the high temperature dynamics of both  $\Delta\sigma$  and  $\Delta R/R$  exhibit oscillatory components (clearly isolated below, in Figs. 4a and 5b) which are direct signatures of acoustic wave propagation, similar to those reported in  $V_2O_3$ <sup>8,9</sup>. Budai *et al.*<sup>28</sup> have observed that strongly anharmonic phonons rather than electronic effects stabilize the metallic phase of  $VO_2$ . The results shown here confirm the strength of electron-phonon coupling in metallic  $VO_2$  since acoustic signatures are seen not only in  $\Delta R/R$ , as expected, but also in  $\Delta\sigma$ , a clear indication that lattice dynamics modulate the Drude response of the system above  $T_{IMT}$ .

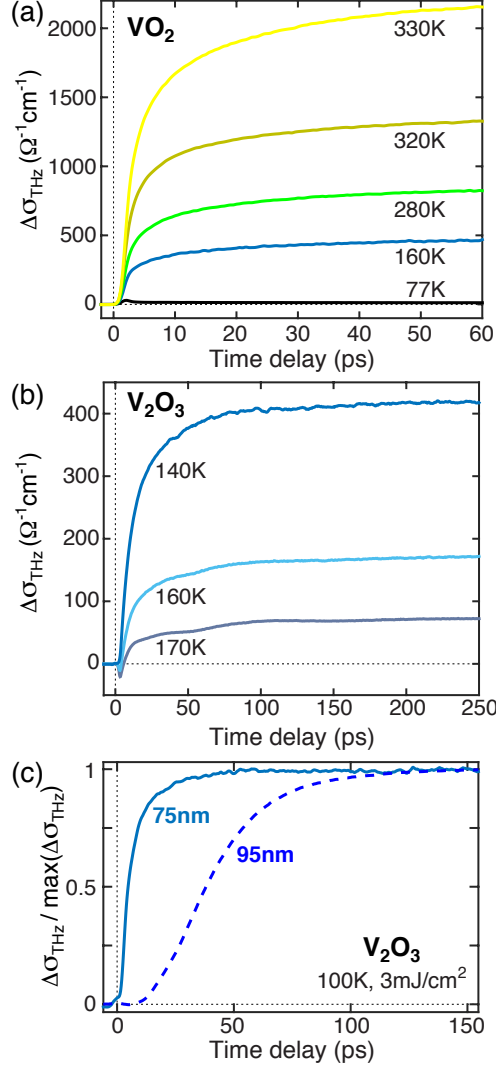


FIG. 2. Transient  $\Delta\sigma$  of (a) 75 nm thick  $\text{VO}_2$ , (b) 75nm thick  $\text{V}_2\text{O}_3$ , and (c) 75 nm and 95 nm thick  $\text{V}_2\text{O}_3$  for temperatures below  $T_{\text{IMT}}$  at a pump fluence of (a)  $3.8 \text{ mJ/cm}^2$ , (b)  $1 \text{ mJ/cm}^2$  and (c)  $3 \text{ mJ/cm}^2$ . Starting in the insulating phase, the THz response consists in a transient conductivity increase which corresponds to the IMT. (c) compares the normalized  $\Delta\sigma(t)$  for the 95 nm and 75 nm  $\text{V}_2\text{O}_3$  films at 100 K, revealing a significant difference in IMT dynamics at short time delays which arises from different defect densities in the films.

### C. Conductivity and reflectivity dynamics in $\text{V}_2\text{O}_3$

As a counterpart to the data on  $\text{VO}_2$ , Figs. 2b, 3c and 3d show  $\Delta\sigma$  and  $\Delta R/R$  for  $\text{V}_2\text{O}_3$  at temperatures below (Fig. 2b) and above (Figs. 3c and 3d)  $T_{\text{IMT}}$  for a pump fluence of

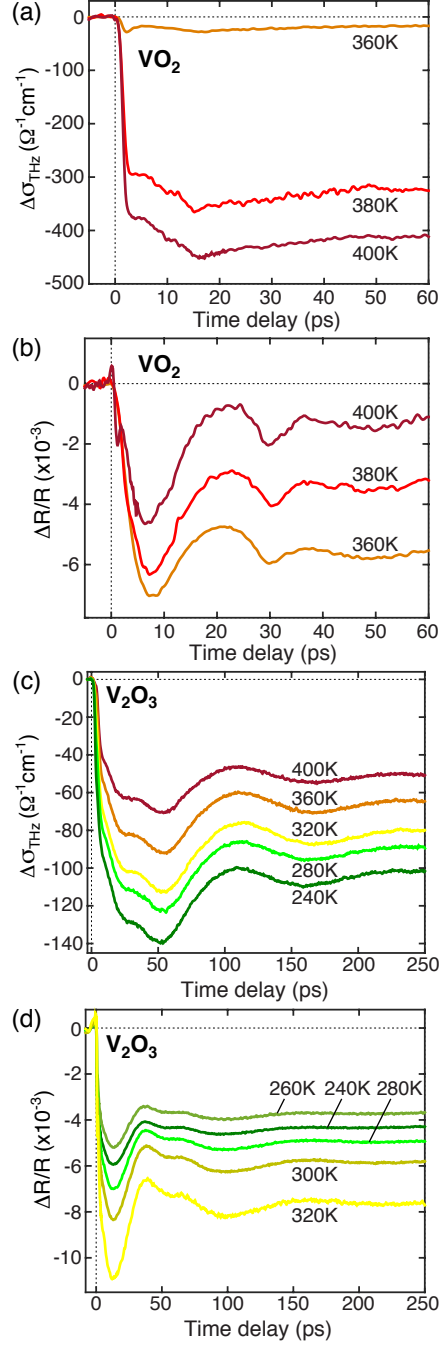


FIG. 3. Transient  $\Delta\sigma$  (a, c) and  $\Delta R/R$  (b, d) of 75 nm thick  $\text{VO}_2$  (a, b) and  $\text{V}_2\text{O}_3$  (c, d) for temperatures above  $T_{IMT}$  at a pump fluence of  $3.8 \text{ mJ/cm}^2$  (a, b) and  $1 \text{ mJ/cm}^2$  (c, d). Shown are the metallic reflectivity responses, dominated by acoustic signatures, and the metallic conductivity responses, also with clear acoustic signatures.

$1 \text{ mJ/cm}^2$ .  $\text{V}_2\text{O}_3$  also exhibits a tens of ps  $\Delta\sigma$  increase characteristic of a percolative IMT

(Fig. 2b). The decrease in  $\Delta\sigma$  with increasing initial temperature stems solely from the fact that temperatures closer to  $T_{IMT}$  are used compared to  $\text{VO}_2$ , so that the initial state already has a finite conductivity (Fig. 1) and the  $\Delta\sigma$  response saturates as the full metallic state is reached. Photoexcitation of the system in the metallic phase at  $T > T_{IMT}$  produces a decrease of both  $\Delta\sigma$  and  $\Delta R/R$  in addition to clearly defined temperature dependent acoustic signatures, as previously reported<sup>8,9</sup>.

Figure 2c compares the normalized  $\Delta\sigma(t)$  for the 95 nm and 75 nm  $\text{V}_2\text{O}_3$  films at 100 K for a pump fluence of 3 mJ/cm<sup>2</sup>. The 95 nm film has a metallic conductivity more than twice as large as the 75 nm film (Fig. 1b and Fig. S2<sup>34</sup>), which is likely due to its single crystalline rather than polycrystalline nature and to its consequent smaller defect density. As discussed in an earlier publication<sup>50</sup>, the defect density has a strong influence not only on the static properties but also on the transition dynamics of  $\text{V}_2\text{O}_3$  thin films since it affects the nucleation and growth of metallic domains in the insulating phase. For  $\text{V}_2\text{O}_3$  and  $\text{VO}_2$ , it is important to distinguish between ultrafast transition dynamics that occur at the microscopic level, independent of the nucleation and growth process, and those that occur at the mesoscopic level where the response is dominated by nucleation and growth. Microscopic effects have been extensively discussed, particularly in the case of  $\text{VO}_2$ <sup>23,35,51,52</sup>. Using a THz probe, which is sensitive to the mesoscale dynamics, we observe fast  $\Delta\sigma(t)$  transients that start during photoexcitation by the pump pulse for the 75 nm film, whereas the 95 nm film exhibits slower variations and a delayed onset relative to the pump arrival time (Fig. 2c). These significant differences in conductivity dynamics cannot be explained by the minimal difference in film thickness. Rather, they occur due to the 95 nm film containing fewer defects than the 75 nm film, and hence fewer defect-induced preferential nucleation sites, which slows down the photoinduced IMT in the thicker sample<sup>50</sup>. Such mesoscopic effects occur independently in addition to any microscopic modifications, and their effect on the dynamics must be taken into account in studies of both  $\text{V}_2\text{O}_3$  and  $\text{VO}_2$ .

#### D. Acoustic dynamics – dependence on film thickness and temperature

Despite differences in IMT timescales (Figs. 2c and S5<sup>34</sup>), high temperature dynamic data for the 50 nm  $\text{VO}_2$  film and the 95 nm  $\text{V}_2\text{O}_3$  film are comparable to the 75 nm films of each material and consequently are shown in Fig. S4 of the Supplemental Material<sup>34</sup>.

Finally,  $\Delta R/R$  dynamics for  $\text{VO}_2$  and  $\text{V}_2\text{O}_3$  at  $T < T_{IMT}$  also exhibit acoustic oscillations characteristic of the insulating phase. The full  $\Delta R/R$  dynamic insulating responses have many contributing factors and are therefore less straightforward to analyze than the metallic responses. As the present work focuses on the acoustic component, the full low temperature  $\Delta R/R$  signals are shown in Fig. S3<sup>34</sup>. The acoustic signatures of the insulating phase can, however, be compared with the metallic phase results of Figs. 3b and 3d, as shown in Fig. 5 and discussed in Section IV below.

#### IV. ANALYSIS AND DISCUSSION

In order to analyze the acoustic dynamics in more detail, we subtract all exponential non-oscillatory contributions to the metallic data in Fig. 3, as detailed in the Supplemental Material<sup>34</sup>. These exponential components of the dynamics, due to nonlinear electronic responses and to thermal decay, are consistent with previously reported measurements<sup>7-9,13,16,53,54</sup> but their detailed discussion is beyond the scope of our present work. Background subtraction yields the acoustic contribution to  $\Delta\sigma(t)$ , shown in Fig. 4, and to the  $\Delta R/R$  dynamics, shown in Fig. 5. The lack of acoustic signatures in the insulating phase  $\Delta\sigma(t)$  response in Figs. 2a and 2b is expected since the THz probe is only sensitive to the metallic volume fraction<sup>50</sup>.

##### A. Transient acoustic modulation of the THz conductivity

The acoustic component of the  $\Delta\sigma$  dynamics is shown in Fig. 4a and 4b for  $\text{VO}_2$  and  $\text{V}_2\text{O}_3$ , respectively. The modulation is significantly longer lived in  $\text{V}_2\text{O}_3$ , an indication that phonon damping is smaller in  $\text{V}_2\text{O}_3$  than in  $\text{VO}_2$ . The significance of phonon damping for the properties of  $\text{VO}_2$  and  $\text{V}_2\text{O}_3$  will be discussed in more detail below.

In Fig. 4c, the maximum  $\Delta\sigma$  oscillation amplitude for both  $\text{VO}_2$  and  $\text{V}_2\text{O}_3$  is plotted as a function of  $T - T_{IMT}$ . The maximum is estimated at the time delays marked by vertical gray bars in Figs. 4a and 4b to avoid potential residual contributions from non-acoustic effects at shorter time delays. The choice of temperature scale enables a direct comparison between the different samples and materials. The bottom part of Fig. 4c shows the oscillation amplitude maxima normalized by the static conductivity at that temperature<sup>34</sup>, while the

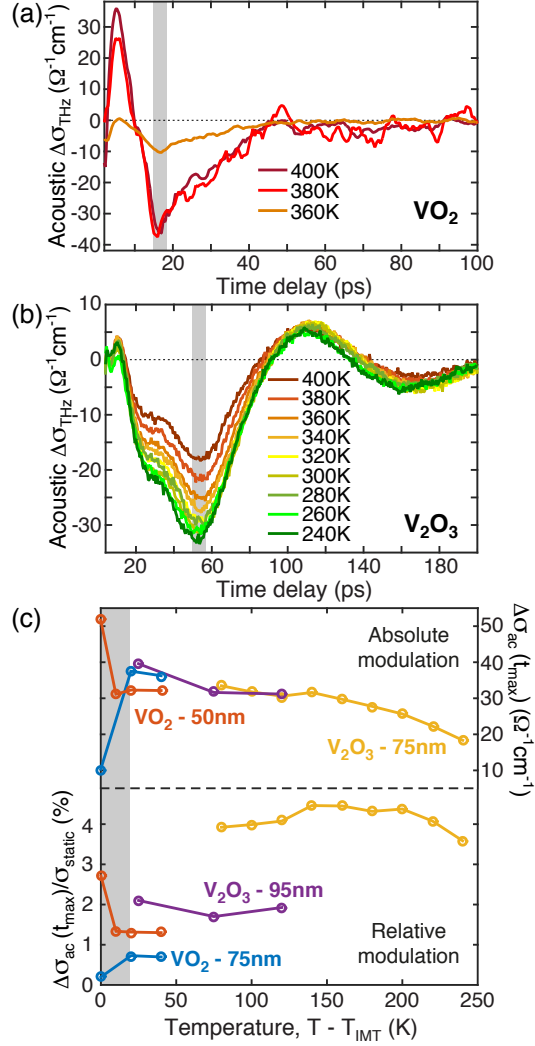


FIG. 4. Background subtracted  $\Delta\sigma$  acoustic oscillations for (a) VO<sub>2</sub> and (b) V<sub>2</sub>O<sub>3</sub>, corresponding to the data from Figs. 3a and 3c.  $\Delta\sigma(t)$  data for the VO<sub>2</sub> film were smoothed using a five point (1 ps) moving average. Vertical gray bars indicate the time delays at which the values in (c) were calculated<sup>34</sup>. (c) Bottom: Temperature dependence of the maximum acoustic modulation of  $\Delta\sigma$ , normalized by the static conductivity at the corresponding temperature (Figs. 1 and S2<sup>34</sup>). Top: Temperature dependence of the maximum acoustic modulation of  $\Delta\sigma$ . Data is shown for all four VO<sub>2</sub> and V<sub>2</sub>O<sub>3</sub> films. A fluence of 3.8 mJ/cm<sup>2</sup> was used for the 75 nm thick VO<sub>2</sub> film (blue), 4 mJ/cm<sup>2</sup> for the 50 nm VO<sub>2</sub> (orange), 1 mJ/cm<sup>2</sup> for the 75 nm V<sub>2</sub>O<sub>3</sub> (yellow) and 3 mJ/cm<sup>2</sup> for the 95 nm V<sub>2</sub>O<sub>3</sub> (purple). The gray shaded region corresponds to temperatures  $T < T_{\text{IMT}} + 20$  K, where the influence of the IMT hysteresis could affect the results.

top shows the non-normalized values. For  $T > T_{IMT} + 20$  K, i.e. well outside the hysteresis region (Fig. 1), the absolute value of the maximum conductivity modulation (top of Fig. 4c) decreases with increasing temperature for all films. This decrease is consistent with the negative slope of the static conductivity observed with increasing temperature in the metallic phase (Figs. 1 and S2<sup>34</sup>). Interestingly, the conductivity oscillation amplitudes are very similar for all the samples examined, even after accounting for the differences in pump fluence (the fluence dependence for the two  $V_2O_3$  samples is discussed in Section II F and Fig. S6 of the Supplemental Material<sup>34</sup>). In particular, oscillation amplitudes are comparable for  $VO_2$  and  $V_2O_3$ , as well as for samples of the same material with different static conductivities.

The normalized plot in Fig. 4c (bottom) enables a more direct comparison of  $VO_2$  and  $V_2O_3$  results **since it provides a measure of the effective acoustic modulation, independent of the overall conductivity of the sample**. It is clear that acoustic modulations in the 75 nm thick  $V_2O_3$  are stronger than in  $VO_2$ , which points to larger electron-phonon induced strain modulation. This conclusion is further strengthened if the different pump fluences are taken into account when analyzing the data (cf. Section II F and Fig. S6 of the Supplemental Material<sup>34</sup>). The 95 nm thick  $V_2O_3$  film does not show such a strikingly higher effect compared to  $VO_2$ . **This could be due to lower acoustic impedance between sample and substrate in this 95 nm  $V_2O_3$  film, the only single crystalline system among all epitaxial films under study, which would cause a decrease in the amplitude of acoustic modulations.** The normalized plot of Fig. 4c also shows that the effective acoustic modulation displays **no clear dependence on temperature.**

### **B. Acoustic modulation of $\Delta R/R$ – temperature dependence of the sound velocity**

It is not trivial to relate the acoustic oscillation period in  $\Delta\sigma(t)$  with the sound velocity in the system since the THz probe, with its  $\sim 300$   $\mu\text{m}$  wavelength, effectively probes an average acoustic modulation of the conductivity in the sub-micron thick films<sup>9</sup>. However, an approximate sound velocity value can be directly determined using oscillations of  $\Delta R/R$ , the transient reflectivity at 800 nm<sup>42</sup>. A model of the  $\Delta R/R$  response expected for a strain modulated thin film following photoexcitation is given in Section III and Fig. S7 of the Supplemental Material<sup>34</sup>. The success of this model in reproducing the data on a thicker

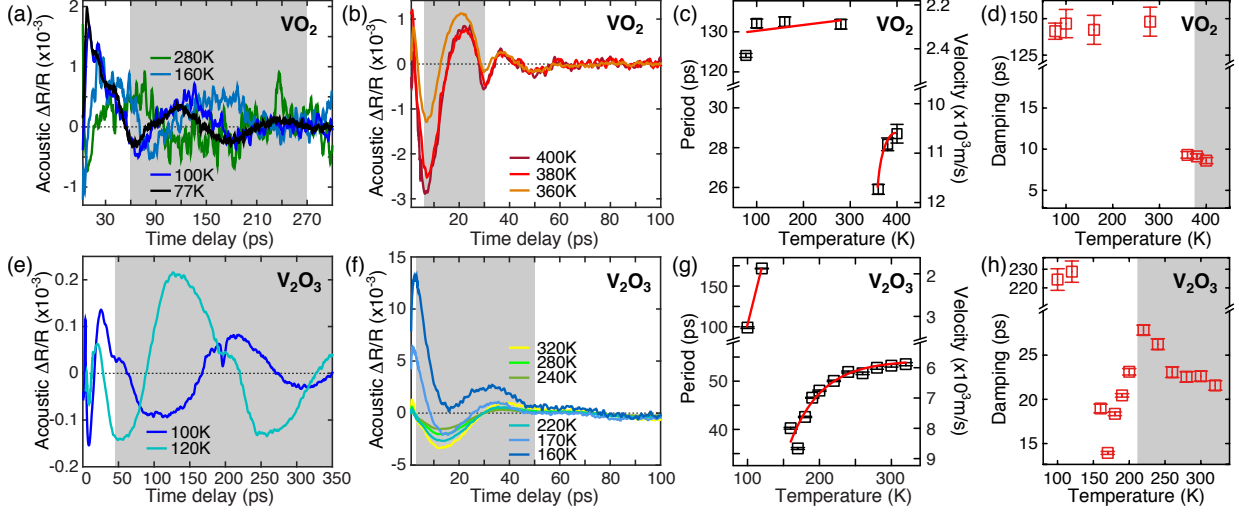


FIG. 5. Background subtracted  $\Delta R/R$  acoustic oscillations for (a) insulating and (b) metallic  $\text{VO}_2$  and for (e) insulating and (f) metallic  $\text{V}_2\text{O}_3$ , corresponding to the data in Figs. 3b, 3d and S3<sup>34</sup>. Plots to the right show the temperature dependence of the acoustic oscillation period and the corresponding sound velocity (c, g), as well as of the damping time (d, h), for  $\text{VO}_2$  (c, d) and for  $\text{V}_2\text{O}_3$  (f, h), extracted by fitting the shaded regions of a, b, e and f with a damped sinusoid. Red lines in c and g are linear fits (c, g: insulating phase), an exponential guide to the eye (c: metallic phase) and an exponential fit (g: metallic phase). In d and h the fully metallic region is shaded gray, for comparison with Fig. 1.

$\text{V}_2\text{O}_3$  film serves as a validation of the use of  $\Delta R/R$  oscillations to extract sound velocity values.

We focus on the acoustic oscillations which are isolated in Fig. 5, obtained from the data in Figs. 3b and 3d for  $T > T_{IMT}$ , and in Fig. S3<sup>34</sup> for  $T < T_{IMT}$ . Acoustic modulations of  $\Delta R/R$  for  $T < T_{IMT}$  are more difficult to observe in  $\text{V}_2\text{O}_3$  than in  $\text{VO}_2$  as the current measurements are limited to temperatures above 80 K. Indeed, the lower value of  $T_{IMT}$  for  $\text{V}_2\text{O}_3$  compared to  $\text{VO}_2$ , as well as the fact that the latent heat is smaller and therefore the IMT can be driven at the same fluence for lower temperatures relative to  $T_{IMT}$ , means that the acoustic response of the insulating phase in  $\text{V}_2\text{O}_3$  is quickly masked by phase transition dynamics. This problem could be circumvented in future work by analyzing the response at lower temperatures or by studying doped  $\text{V}_2\text{O}_3$  samples.

The period of the reflectivity oscillations shown in Figs. 5c and 5g is determined by

fitting the shaded regions in the corresponding reflectivity data with a damped sinusoid,  $\Delta R = \Delta R_0 + A \times \exp(-t/t_d) \times \sin(2\pi(t - t_0)/\tau)$ , where  $\tau$  is the period and  $t_d$  the damping time. The fidelity of the fit is validated by the near unity adjusted  $R^2$  values (cf. Section II D of the Supplemental Material<sup>34</sup>). Given that the 75 nm thickness of the films is on the order of acoustic phonon wavelengths<sup>40</sup>, the observed oscillations are essentially reflections of the acoustic wave between the film surface and the film-substrate interface, as described in Section I. The corresponding sound velocity can therefore be calculated from the period,  $\tau$ , using  $v_{sound} = 4d/\tau$ <sup>41,42</sup>, where  $d$  is the film thickness.

The most striking effect in these data is that the sound velocity associated with these oscillations, apart from a slow and monotonic increase with temperature, exhibits an abrupt increase at  $T_{IMT}$  when going from the insulating to the metallic phase, by a factor of 4-5 in  $\text{VO}_2$  and 3-5 in  $\text{V}_2\text{O}_3$ . This is seen clearly in Figs. 5c and 5g. Such a large sound velocity variation is not unexpected in vanadium oxides, where lattice constants change by about 1% across the structural phase transition that accompanies the IMT<sup>34,37,55</sup>. V-O and V-V bond lengths change by up to 4% across the structural transition, on average, stabilizing an insulating phase below  $T_{IMT}$  or a metallic phase above  $T_{IMT}$ <sup>33,34,56</sup>.

Previous sound velocity measurements for the metallic phase of  $\text{VO}_2$  **bulk single crystals** yield approximately  $4 \times 10^3$  m/s, measured along the rutile c-axis for surface Rayleigh waves by Maurer *et al.*<sup>26</sup>, or  $8 \times 10^3$  m/s, determined from the phonon dispersion of the longitudinal acoustic mode along the  $\Gamma$ -Z direction in Budai *et al.*<sup>28</sup>. In the metallic phase of  $\text{V}_2\text{O}_3$  Seikh *et al.*<sup>40</sup> and Yelon *et al.*<sup>57</sup> report  $8 \times 10^3$  m/s, corresponding to longitudinal acoustic mode propagation. The  $\text{VO}_2$  and  $\text{V}_2\text{O}_3$  metallic sound velocities shown in Fig. 5 are consistent with the order of magnitude reported previously. Maurer *et al.*<sup>26</sup> and Seikh *et al.*<sup>40</sup> also measure the sound velocity across the IMT, for  $\text{VO}_2$  and  $\text{V}_2\text{O}_3$ , respectively, and find variations by a factor of at most 1.5, smaller than the one we report in this work. **We note, however, that these previous measurements were performed on bulk samples while our current results correspond to thin film properties. Some difference in the absolute value of the sound velocity as well as in its variation across the IMT is expected between bulk and thin film samples, as discussed below. Our work quantifies this difference using a method which can easily be extended to other systems.**

Sample to sample variation in vanadium oxides, and in particular in vanadium oxide thin films, is well known and must be taken into account when analyzing and comparing

different data sets<sup>39</sup>. In particular, variation in sound velocity values is a result of the different strain environments and crystallinity of the samples. The strain sensitivity of VO<sub>2</sub> material properties, in particular, is widely reported<sup>39,58–61</sup> and is caused by large differences in lattice constant values along different crystallographic axes with large variations of these values across the IMT (Table SI<sup>34</sup>). For the measurements presented here, sound velocity determination could be affected by acoustic waves propagating at an angle to the film normal, by substrate-induced strain in the growth direction, as well as by contributions from other acoustic modes in the system, in particular non-longitudinal waves.

### C. Increased phonon damping in the metallic phase

Analyzing Figs. 4a and 4b and Figs. 5b and 5f from the perspective of acoustic modulation damping reveals that the amplitude of the metallic phase  $\Delta\sigma$  and  $\Delta R/R$  oscillations decays faster in VO<sub>2</sub> than in V<sub>2</sub>O<sub>3</sub>. The damped sinusoid fit to the metallic  $\Delta R/R$  data yields damping times of about 10 ps for VO<sub>2</sub> (Fig. 5d) and 20 ps for V<sub>2</sub>O<sub>3</sub> (Fig. 5h)<sup>34</sup>. Damping effects are thus stronger in the metallic phase of VO<sub>2</sub> compared to V<sub>2</sub>O<sub>3</sub>. The observations from Budai *et. al.*<sup>28</sup> of increased phonon damping in the metallic phase compared to the insulating phase are verified by our analysis on VO<sub>2</sub>, where the damping time decreases from 145 ps in the insulator to 10 ps in the metal. The results for V<sub>2</sub>O<sub>3</sub> show a decrease in damping time from 225 ps in the insulating phase to 20 ps in the metallic phase, suggesting a similar influence of phonon anharmonicity to be at play in the metallic phase of V<sub>2</sub>O<sub>3</sub>. It should be noted that an additional source of damping exists, due to transmission of the acoustic wave into the substrate. Transmission losses will depend on how well acoustic impedances are matched between the film and the substrate, and can potentially lead to an increased effective damping time associated with the VO<sub>2</sub> or V<sub>2</sub>O<sub>3</sub> material responses alone. Quantitative comparisons with damping times obtained from other methods must therefore be done with care. Details of the damping analysis are presented in Section II D of the Supplemental Material<sup>34</sup>.

### D. Discussion

Figures 4 and 5 provide a measure of photoinduced acoustic signatures in  $\text{VO}_2$  and  $\text{V}_2\text{O}_3$ . It is interesting to compare the temperature dependence of the different properties of the system. While the static conductivity, sound velocity and acoustic damping all vary with temperature in the metallic phase, the effective acoustic modulation (normalized plot at the bottom of Fig. 4c) shows no clear temperature dependence.

Comparing  $\text{VO}_2$  and  $\text{V}_2\text{O}_3$  in Figures 4 and 5 enables us to conclude that acoustic signatures are qualitatively the same and quantitatively within a factor of two of each other. This is so despite differences in the mechanism that drives the IMT, in particular the larger effect expected from electronic correlations in  $\text{V}_2\text{O}_3$  compared to  $\text{VO}_2$ , and in the latent heat associated with the IMT (65 J/cm<sup>3</sup> for  $\text{V}_2\text{O}_3$ <sup>62</sup> and 240 J/cm<sup>3</sup> for  $\text{VO}_2$ <sup>63</sup>). In the remainder of the manuscript we discuss the possible origin of the larger acoustic modulation signal that is observed for  $\text{V}_2\text{O}_3$ . First, the electron-phonon coupling coefficient is higher for  $\text{V}_2\text{O}_3$  ( $3 \times 10^{18}$  W K<sup>-1</sup>m<sup>-3</sup><sup>34</sup>) than for  $\text{VO}_2$  ( $10^{18}$  W K<sup>-1</sup>m<sup>-3</sup><sup>64</sup>), which partially explains the increased signal strength since energy couples more efficiently between the electrons and the lattice. This means that the strain wave generation process following electronic photoexcitation is more efficient in  $\text{V}_2\text{O}_3$ , and that the subsequent strain-induced modifications of the electronic spectral weight are stronger. In fact, metallic  $\text{V}_2\text{O}_3$  at atmospheric conditions is seen to lie near a transition line to a pressure induced isostructural paramagnetic insulating phase (Fig. S1), so that one would indeed expect a similar pressure change to lead to a larger change in the conductivity for  $\text{V}_2\text{O}_3$  than for  $\text{VO}_2$ . Second, the lattice structure of  $\text{V}_2\text{O}_3$  is overall more amenable to modulations, as deduced from the lower phonon damping measured in  $\text{V}_2\text{O}_3$  compared to  $\text{VO}_2$  which effectively means that the structure is less rigid. This implies that photoinduced strain modulations would be larger in  $\text{V}_2\text{O}_3$  for the same amount of energy transferred to the lattice. Lastly, it is important to reiterate the strong influence of differences in defect density, which lead to variations in the static and dynamic properties of both  $\text{VO}_2$  and  $\text{V}_2\text{O}_3$  when comparing nominally equivalent samples. In particular, such variations are known to affect the structural response of these materials<sup>32</sup>, and should therefore be taken into account when attempting precise quantitative comparisons.

## V. CONCLUSION

This work demonstrates that strong electron-phonon coupling exists and is responsible for clear ultrafast acoustic modulations of the Drude and optical responses in  $V_2O_3$  and  $VO_2$ . This effect appears to be stronger for  $V_2O_3$  than for  $VO_2$ , suggesting that the electronic and lattice structures of  $V_2O_3$  are more amenable to transient strain modulation than those of  $VO_2$ .

We further identify a significant temperature dependence of the sound velocity in both materials, in particular a dramatic increase by a factor of 4-5 in  $VO_2$  and 3-5 in  $V_2O_3$  across the IMT. The observation (in both materials) of stronger acoustic damping in the metallic phase relative to the insulating one confirms the strong role of phonon anharmonicity in metallic  $VO_2$  and suggests that a similar mechanism is at play in  $V_2O_3$ . The timescale for damping of the acoustic modulations in both the THz conductivity (Drude response) and the near infrared reflectivity (spectral weight at 1.55 eV, related to the occupation of  $V3d$  orbitals) are longer for  $V_2O_3$  than for  $VO_2$ , indicating stronger damping in the latter and thus a potentially stronger phonon anharmonicity contribution.

Our findings demonstrate that transient strain induced by photoexcitation is a useful tool to both analyze and control the electronic properties of complex materials and their coupling to lattice excitations. The same approach could be used to investigate the modifications to the electronic and lattice properties induced by different defect densities. This is particularly relevant in the case of  $VO_2$  and  $V_2O_3$ , where different defect densities lead to strong sample to sample variation of static and dynamic properties, but is likely applicable to other complex materials and to their properties which are characteristically sensitive to small perturbations.

## VI. ACKNOWLEDGEMENTS

We thank Mariano Trigo and Gabriel Lantz for useful discussions.

E. A. acknowledges support from the ETH Zurich Postdoctoral Fellowship Program and from the Marie Curie Actions for People COFUND Program. R. D. A. and E. A. acknowledges support from DOE—Basic Energy Sciences under Grant No. DE-FG02-09ER46643. S. J. Y. and H.-T. K. acknowledge support from the MIT project at ETRI. I. K. S., S. W., J. G. R. and K. W. acknowledge support from AFOSR under Grant No. FA9550-16-1-0026 One of

us (I.K.S.) acknowledges support from the Vannevar Bush Faculty Fellowship program sponsored by the Basic Research Office of the Assistant Secretary of Defense for Research and Engineering and funded by the Office of Naval Research through grant N00014-15-1-2848. J. G. R. kindly acknowledges support from FAPA program through Facultad de Ciencias and Vicerrectoria de Investigaciones of Universidad de los Andes, Bogotá, Colombia, and Colciencias No. 120471250659.

---

\* elsabreu@phys.ethz.ch. Previously at Department of Physics, Boston University, Boston MA 02215, USA

† Previously at Department of Physics, Boston University, Boston MA 02215, USA

‡ mengkun.liu@stonybrook.edu. Previously at Department of Physics, Boston University, Boston MA 02215, USA

§ raveritt@physics.ucsd.edu. Previously at Department of Physics, Boston University, Boston MA 02215, USA

<sup>1</sup> M. Hashimoto, E. A. Nowadnick, R.-H. He, I. M. Vishik, B. Moritz, Y. He, K. Tanaka, R. G. Moore, D. Lu, Y. Yoshida, M. Ishikado, T. Sasagawa, K. Fujita, S. Ishida, S. Uchida, H. Eisaki, Z. Hussain, T. P. Devereaux, and Z.-X. Shen, *Nature Materials* **14**, 37 (2014).

<sup>2</sup> S. Jin, T. H. Tiefel, M. McCormack, R. A. Fastnacht, R. Ramesh, and L. H. Chen, *Science* **264**, 413 (1994).

<sup>3</sup> T. Kubacka, J. A. Johnson, M. C. Hoffmann, C. Vicario, S. de Jong, P. Beaud, S. Grübel, S.-W. Huang, L. Huber, L. Patthey, Y.-D. Chuang, J. J. Turner, G. L. Dakovski, W.-S. Lee, M. P. Minitti, W. Schlotter, R. G. Moore, C. P. Hauri, S. M. Koohpayeh, V. Scagnoli, G. Ingold, S. L. Johnson, and U. Staub, *Science* **343**, 1333 (2014).

<sup>4</sup> Y. H. Wang, H. Steinberg, P. Jarillo-Herrero, and N. Gedik, *Science* **342**, 453 (2013).

<sup>5</sup> R. D. Averitt and A. J. Taylor, *Journal of Physics: Condensed Matter* **14**, R1357 (2002).

<sup>6</sup> J. Orenstein, *Physics Today* **65**, 44 (2012).

<sup>7</sup> O. V. Misochko, M. Tani, K. Sakai, K. Kisoda, S. Nakashima, V. N. Andreev, and F. A. Chudnovsky, *Physical Review B* **58**, 12789 (1998).

<sup>8</sup> B. Mansart, D. Boschetto, S. Sauvage, A. Rousse, and M. Marsi, *Europhysics Letters* **92**, 37007 (2010).

- <sup>9</sup> M. Liu, B. Pardo, J. Zhang, M. M. Qazilbash, S. J. Yun, Z. Fei, J. H. Shin, H.-T. Kim, D. N. Basov, and R. D. Averitt, *Physical Review Letters* **107**, 066403 (2011).
- <sup>10</sup> F. Rodolakis, P. Hansmann, J. P. Rueff, A. Toschi, M. W. Haverkort, G. Sangiovanni, A. Tanaka, T. Saha-Dasgupta, O. K. Andersen, K. Held, M. Sikora, I. Alliot, J. P. Itié, F. Baudelet, P. Wzietek, P. Metcalf, and M. Marsi, *Physical Review Letters* **104**, 047401 (2010).
- <sup>11</sup> A. Cavalleri, C. Tóth, C. W. Siders, J. A. Squier, F. Ráksi, P. Forget, and J. C. Kieffer, *Physical Review Letters* **87**, 237401 (2001).
- <sup>12</sup> M. A. Huber, M. Plankl, M. Eisele, R. E. Marvel, F. Sandner, T. Korn, C. Schller, J. R. F. Haglund, R. Huber, and T. L. Cocker, *Nano Letters* **16**, 1421 (2016).
- <sup>13</sup> B. T. O’Callahan, A. C. Jones, J. Hyung Park, D. H. Cobden, J. M. Atkin, and M. B. Raschke, *Nature Communications* **6**, 6849 (2015).
- <sup>14</sup> G. Lantz, B. Mansart, D. Grieger, D. Boschetto, N. Nilforoushan, E. Papalazarou, N. Moisan, L. Perfetti, V. L. R. Jacques, D. L. Bolloc’h, C. Laulhé, S. Ravy, J. P. Rueff, T. E. Glover, M. P. Hertlein, Z. Hussain, S. Song, M. Chollet, M. Fabrizio, and M. Marsi, *Nature Communications* **8**, 13917 (2017).
- <sup>15</sup> S. Wang, J. G. Ramírez, J. Jeffet, S. Bar-Ad, D. Huppert, and I. K. Schuller, *Europhysics Letters* **118**, 27005 (2017).
- <sup>16</sup> A. Pashkin, C. Kübler, H. Ehrke, R. Lopez, A. Halabica, R. F. Haglund, R. Huber, and A. Leitenstorfer, *Physical Review B* **83**, 195120 (2011).
- <sup>17</sup> D. Wegkamp, M. Herzog, L. Xian, M. Gatti, P. Cudazzo, C. L. McGahan, R. E. Marvel, R. F. Haglund, A. Rubio, M. Wolf, and J. Stähler, *Physical Review Letters* **113**, 216401 (2014).
- <sup>18</sup> A. X. Gray, M. C. Hoffmann, J. Jeong, N. P. Aetukuri, D. Zhu, H. Y. Hwang, N. C. Brandt, H. Wen, A. J. Sternbach, S. Bonetti, A. H. Reid, R. Kukreja, C. E. Graves, T. Wang, P. W. Granitzka, Z. Chen, D. J. Higley, T. Chase, E. Jal, E. Abreu, M. Liu, T.-C. Weng, D. Sokaras, D. Nordlund, M. Chollet, H. T. Lemke, J. Glowonia, M. Trigo, Y. Zhu, H. Ohldag, J. W. Freeland, M. G. Samant, J. Berakdar, R. D. Averitt, K. A. Nelson, S. S. P. Parkin, and H. A. Dürr, *arXiv*, 1601.07490 (2016).
- <sup>19</sup> F. J. Morin, *Physical Review Letters* **3**, 34 (1959).
- <sup>20</sup> D. B. McWhan, T. Rice, and J. P. Remeika, *Physical Review Letters* **23**, 1384 (1969).
- <sup>21</sup> D. B. McWhan, J. P. Remeika, T. M. Rice, W. F. Brinkman, J. P. Maita, and A. Menth, *Physical Review Letters* **27**, 941 (1971).

- <sup>22</sup> P. Baum, D.-S. Yang, and A. H. Zewail, *Science* **318**, 788 (2007).
- <sup>23</sup> M. M. Qazilbash, A. A. Schafgans, K. S. Burch, S. J. Yun, B. G. Chae, B. J. Kim, H.-T. Kim, and D. N. Basov, *Physical Review B* **77**, 115121 (2008).
- <sup>24</sup> P. Pfalzer, G. Obermeier, M. Klemm, S. Horn, and M. L. DenBoer, *Physical Review B* **73**, 144106 (2006).
- <sup>25</sup> P. Limelette, A. Georges, D. Jérôme, P. Wzietek, P. Metcalf, and J. M. Honig, *Science* **302**, 89 (2003).
- <sup>26</sup> D. Maurer, A. Leue, R. Heichele, and V. Müller, *Physical Review B* **60**, 13249 (1999).
- <sup>27</sup> L. Baldassarre, A. Perucchi, D. Nicoletti, A. Toschi, G. Sangiovanni, K. Held, M. Capone, M. Ortolani, L. Malavasi, M. Marsi, P. Metcalf, P. Postorino, and S. Lupi, *Physical Review B* **77**, 113107 (2008).
- <sup>28</sup> J. D. Budai, J. Hong, M. E. Manley, E. D. Specht, C. W. Li, J. Z. Tischler, D. L. Abernathy, A. H. Said, B. M. Leu, L. A. Boatner, R. J. McQueeney, and O. Delaire, *Nature* **515**, 535 (2014).
- <sup>29</sup> Z. Tao, T.-R. Han, S. Mahanti, P. Duxbury, F. Yuan, C.-Y. Ruan, K. Wang, and J. Wu, *Physical Review Letters* **109**, 166406 (2012).
- <sup>30</sup> V. R. Morrison, R. P. Chatelain, K. L. Tiwari, A. Hendaoui, A. Bruháes, M. Chaker, and B. J. Siwick, *Science* **346**, 445 (2014).
- <sup>31</sup> A. X. Gray, J. Jeong, N. P. Aetukuri, P. Granitzka, Z. Chen, R. Kukreja, D. Higley, T. Chase, A. H. Reid, H. Ohldag, M. A. Marcus, A. Scholl, A. T. Young, A. Doran, C. A. Jenkins, P. Shafer, E. Arenholz, M. G. Samant, S. S. P. Parkin, and H. A. Dürr, *Physical Review Letters* **116**, 116403 (2016).
- <sup>32</sup> J. G. Ramírez, T. Saerbeck, S. Wang, J. Trastoy, M. Malnou, J. Lesueur, J.-P. Crocombette, J. E. Villegas, and I. K. Schuller, *Physical Review B* **91**, 205123 (2015).
- <sup>33</sup> M. Marezio, D. B. McWhan, J. P. Remeika, and P. D. Dernier, *Physical Review B* **5**, 2541 (1972).
- <sup>34</sup> See Supplemental Material at ? for (i) a summary of material properties, (ii) raw data and technical analysis details, and (iii) complementary data.
- <sup>35</sup> D. J. Hilton, R. P. Prasankumar, S. Fourmaux, A. Cavalleri, D. Brassard, M. A. El Khakani, J. C. Kieffer, A. J. Taylor, and R. D. Averitt, *Physical Review Letters* **99**, 226401 (2007).
- <sup>36</sup> S. Lysenko, V. Vikhnin, A. Rúa, F. Fernández, and H. Liu, *Physical Review B* **82**, 205425

- (2010).
- <sup>37</sup> D. B. McWhan and J. P. Remeika, *Physical Review B* **2**, 3734 (1970).
- <sup>38</sup> P. B. Allen, *Physical Review Letters* **59**, 1460 (1987).
- <sup>39</sup> M. Liu, A. J. Sternbach, M. Wagner, T. V. Slusar, T. Kong, S. L. Bud'ko, S. Kittiwatanakul, M. M. Qazilbash, A. McLeod, Z. Fei, E. Abreu, J. Zhang, M. Goldflam, S. Dai, G.-X. Ni, J. Lu, H. A. Bechtel, M. C. Martin, M. B. Raschke, R. D. Averitt, S. A. Wolf, H.-T. Kim, P. C. Canfield, and D. N. Basov, *Physical Review B* **91**, 245155 (2015).
- <sup>40</sup> M. M. Seikh, C. Narayana, A. K. Sood, P. Murugavel, M. W. Kim, P. A. Metcalf, J. M. Honig, and C. N. R. Rao, *Solid State Communications* **138**, 466 (2006).
- <sup>41</sup> S. Ge, X. Liu, X. Qiao, Q. Wang, Z. Xu, J. Qiu, P.-H. Tan, J. Zhao, and D. Sun, *Scientific Reports* **4**, 5722 (2014).
- <sup>42</sup> C. Thomsen, J. Strait, Z. Vardeny, H. J. Maris, J. Tauc, and J. J. Hauser, *Physical Review Letters* **53**, 989 (1984).
- <sup>43</sup> C. Thomsen, H. T. Grahn, H. J. Maris, and J. Tauc, *Physical Review B* **34**, 4129 (1986).
- <sup>44</sup> K. G. West, J. Lu, J. Yu, D. Kirkwood, W. Chen, Y. Pei, J. Claassen, and S. A. Wolf, *Journal of Vacuum Science & Technology A* **26**, 133 (2008).
- <sup>45</sup> S. J. Yun, J. W. Lim, J. S. Noh, B. J. Kim, and H. T. Kim, *Japanese Journal of Applied Physics* **48**, 04C139 (2009).
- <sup>46</sup> S. Kittiwatanakul, *Study of metal-insulator transition in strongly correlated vanadium dioxide thin films*, Ph.D. thesis, University of Virginia (2014), section 2.3.2.
- <sup>47</sup> M. M. Qazilbash, K. S. Burch, D. Whisler, D. Shrekenhamer, B. G. Chae, H.-T. Kim, and D. N. Basov, *Physical Review B* **74**, 205118 (2006).
- <sup>48</sup> D. N. Basov, R. D. Averitt, D. Van Der Marel, M. Dressel, and K. Haule, *Reviews of Modern Physics* **83**, 471 (2011).
- <sup>49</sup> M. K. Stewart, D. Brownstead, S. Wang, K. G. West, J. G. Ramírez, M. M. Qazilbash, N. B. Perkins, I. K. Schuller, and D. N. Basov, *Physical Review B* **85**, 205113 (2012).
- <sup>50</sup> E. Abreu, S. Wang, J. G. Ramírez, M. Liu, J. Zhang, K. Geng, I. K. Schuller, and R. D. Averitt, *Physical Review B* **92**, 085130 (2015).
- <sup>51</sup> M. K. Liu, M. Wagner, E. Abreu, S. Kittiwatanakul, A. McLeod, Z. Fei, M. Goldflam, S. Dai, M. M. Fogler, J. Lu, S. A. Wolf, R. D. Averitt, and D. N. Basov, *Physical Review Letters* **111**, 096602 (2013).

- <sup>52</sup> S. A. Dönges, O. Khatib, B. T. OCallahan, J. M. Atkin, J. H. Park, D. Cobden, and M. B. Raschke, *Nano Letters* **16**, 3029 (2016).
- <sup>53</sup> A. Cavalleri, T. Dekorsy, H. H. W. Chong, J. C. Kieffer, and R. W. Schoenlein, *Physical Review B* **70**, 161102(R) (2004).
- <sup>54</sup> S. Wang, J. G. Ramírez, J. Jeffet, S. Bar-Ad, D. Huppert, and I. K. Schuller, (2016), submitted to *Europhysics Letters*.
- <sup>55</sup> D. Kucharczyk and T. Niklewski, *Journal of Applied Crystallography* **12**, 370 (1979).
- <sup>56</sup> P. D. Dernier and M. Marezio, *Physical Review B* **2**, 3771 (1970).
- <sup>57</sup> W. B. Yelon and J. E. Keem, *Solid State Communications* **29**, 775 (1979).
- <sup>58</sup> J. B. Goodenough, *Journal of Solid State Chemistry* **3**, 490 (1971).
- <sup>59</sup> J. Wu, Q. Gu, B. S. Guiton, N. P. D. Leon, L. Ouyang, and H. Park, *Nano Letters* **6**, 2313 (2006).
- <sup>60</sup> J. H. Park, J. M. Coy, T. S. Kasirga, C. Huang, Z. Fei, S. Hunter, and D. H. Cobden, *Nature* **400**, 431 (2013).
- <sup>61</sup> S. Kittiwatanakul, S. A. Wolf, and J. Lu, *Applied Physics Letters* **105**, 073112 (2014).
- <sup>62</sup> H. Keer, D. Dickerson, H. Kuwamoto, H. Barros, and J. Honig, *Journal of Solid State Chemistry* **19**, 95 (1976).
- <sup>63</sup> G. Chandrashekhar, H. Barros, and J. Honig, *Materials Research Bulletin* **8**, 369 (1973).
- <sup>64</sup> M. Liu, H. Y. Hwang, H. Tao, A. C. Strikwerda, K. Fan, G. R. Keiser, A. J. Sternbach, K. G. West, S. Kittiwatanakul, J. Lu, S. A. Wolf, F. G. Omenetto, X. Zhang, K. A. Nelson, and R. D. Averitt, *Nature* **487**, 345 (2012).